Journal of Materials Chemistry A

PAPER

View Article Online
View Journal | View Issue

Cite this: J. Mater. Chem. A, 2015, 3, 2407

Inkjet printing of conductive patterns and supercapacitors using a multi-walled carbon nanotube/Ag nanoparticle based ink†

Siliang Wang,[a] Nishuang Liu,*[a] Jiayou Tao,[a] Congxing Yang,[a] Weijie Liu,[a] Yuling Shi,[a] Yumei Wang,[a] Jun Su,[a] Luying Li[a] and Yihua Gao*[ab]

Received 21st October 2014
Accepted 27th November 2014

DOI: 10.1039/c4ta05625f

www.rsc.org/MaterialsA

A multi-walled carbon nanotube (MWCNT) and silver (Ag) nanoparticle ink for inkjet printing was prepared by dispersing MWCNTs and Ag nanoparticles in water with the assistance of sodium dodecylbenzenesulfonate (SDBS). Highly conductive patterns of Ag–MWCNTs were printed on paper using a HP Deskjet 1010 inkjet printer. The patterns showed good stability during the bending test and a low sheet resistance of ~300 Ω sq^{-1} after being printed 50 times. By simply adding manganese dioxide (MnO_2) nanoparticles with a diameter of 60–90 nm into the ink solution, patterned positive electrodes were prepared for asymmetric supercapacitors (ASCs) with filtrated MWCNT negative electrodes. The ASCs exhibit a wide operating potential window of 1.8 V and excellent electrochemical performances, *e.g.* a high energy density of 1.28 mW h cm^{-3} at a power density of 96 mW cm^{-3} and a high retention ratio of ~96.9% of its initial capacitance after 3000 cycles. The inkjet-printing acting as a simple, low-cost, non-contact deposition method can be fully integrated with the fabrication process in current printed electronic devices and has potential applications in energy storage.

Introduction

Technology advances in flexible and wearable/stretchable electronic devices, such as flexible displays,[1] flexible and conformal antenna arrays,[2] electric circuits and chemical sensors,[3] electronic solar cell arrays,[4] radio frequency identification tags,[5] microstructure electrochemical capacitors[6] and so on, have promoted the demand for high-performance flexible conductive patterns.

Usually, in the fabrication of conductive patterns for flexible electronic devices,[7–9] widely used photolithography involves many steps such as etching, electroplating, *etc.* and is time consuming, complicated and expensive. Compared with photolithography, inkjet printing is not only an easy access and low cost non-contact deposition method for obtaining conductive patterns, but also allows us to readily control the pattern geometry, location, electrical conductivity, film thickness and uniformity of the film.[10] Apart from conductive patterns, inkjet printing has many applications, such as thin-film transistors,[11–14] light-emitting devices,[15] solar cells,[16,17] memory and magnetic device applications,[18,19] sensors and detectors,[20,21] and so on. However there have been few reports[22,23] on the production of energy storage devices *via* inkjet printing currently, and the present work addresses this key application.

CNTs have become attractive nanoscale materials in various applications due to their unique properties. CNTs have a highly accessible surface area, both high electrical conductivity and mechanical flexibility as well as high stability and are of low cost,[24] so CNTs are promising materials for supercapacitors and an alternative to conductive electrodes. Nowadays, many research studies are dedicated to conductive patterns by inkjet printing of CNTs.[25–28] But the resistance of printed CNTs on a flexible substrate was too high to be widely used in optoelectronic devices. Both Ag nanowires and sintered Ag nanoparticles have the property of high conductivity,[29,30] but Ag nanoparticles are easier to print without clogging the nozzle. Mixing Ag nanoparticles with graphene could dramatically decrease the sheet resistance,[31] so the mixture of Ag nanoparticles and CNTs may also decrease the sheet resistance without the change of mechanical flexibility.

Due to their high specific capacitance compared to carbon materials, transition metal oxides have been extensively studied in the past decades.[32–35] MnO_2 is the most thoroughly investigated for supercapacitor applications because of its remarkable theoretical specific capacitance (1370 F g^{-1}), natural abundance, low cost and environmental friendliness.[36–38] Being

[a]Center for Nanoscale Characterization & Devices (CNCD), Wuhan National Laboratory for Optoelectronics (WNLO), School of Physics, Huazhong University of Science and Technology (HUST), LuoyuRoad 1037, Wuhan 430074, China. E-mail: gaoyihua@hust.edu.cn; nishuang_liu@foxmail.com

[b]Hubei Collaborative Innovation Center for Advanced Organic Chemical Materials, 368 Youyi Avenue, Wuhan 430062, China

† Electronic supplementary information (ESI) available. See DOI: 10.1039/c4ta05625f

limited by its poor electrical conductivity, MnO_2 has rarely achieved the theoretical specific capacitance in the experiment.[39] The incorporation of MnO_2 into the flexible conductive CNT network can provide a feasible approach to overcome the above limitations. However, according to the equation: $E = 0.5CV^2$ (C is the specific capacitance; and V is the cell voltage), MnO_2 would compromise the specific energy density because of its narrow electrochemical working voltage window (0.8–1.0 V). This challenge could be addressed by fabricating ASCs that consist of two different electrodes,[40,41] *i.e.* MnO_2–Ag–MWCNTs as the anode and filtered MWCNTs as the cathode.

In this work, we demonstrate the fabrication of conductive patterns by inkjet printing the Ag–MWCNT ink. Following that, ASCs were made by assembling the above mentioned MnO_2–Ag–MWCNT anodes and filtered MWCNT cathodes. The ASCs show a wide operating potential window of 1.8 V and excellent electrochemical performances, *e.g.* a high energy density of 1.28 mW h cm^{-3} at a power density of 96 mW cm^{-3} and a high retention ratio of ~96.9% of its initial capacitance after 3000 cycles.

Experimental details

Ag–MWCNT and MnO_2–Ag–MWCNT ink production

For the Ag–MWCNT ink production, 200 mg MWCNT powder (Beijing Boyu Gaoke New Material Technology Co., Ltd), 160 mg Ag nanoparticles (diameter of 20–120 nm, Shanghai Chaowei Nanotechnology Co., Ltd), 200 mg SDBS surfactant and 40 ml distilled water were added to a glass bottle. The mixture was stirred for 30 min to form a uniform solution at room temperature and then the probe was ultrasonicated for 30 min. Afterwards, the Ag–MWCNT ink was obtained. For the MnO_2–Ag–MWCNT ink production, the MnO_2 nanoparticles (60–90 nm) were synthesized by a method similar to that reported in the literature.[42] Typically, 50 mg $KMnO_4$ was dissolved in 30 ml de-ionized water, and then 1 ml ethanol was added drop-wise under stirring. The addition of alcohol led to the formation of a brownish precipitate of MnO_2. After ethanol reduction, the mixtures were continuously stirred for 24 h and then the precipitates were filtered, washed with de-ionized water and alcohol and dried at 60 °C for 24 h. The prepared MnO_2 nanoparticles, 200 mg MWCNT powder, 160 mg Ag nanoparticles, 200 mg SDBS surfactant and 40 ml distilled water were added into a glass bottle, and the next procedure was similar to the preparation of the Ag–MWCNT ink.

Inkjet printing of Ag–MWCNT conductive patterns and MnO_2–Ag–MWCNT positive electrodes. Filtrating MWCNT negative electrodes

The Ag–MWCNT ink was injected into a clean ink cartridge (HP 1010) and printed using an HP Deskjet 1010 inkjet printer. In order to deposit a large number of MWCNTs, the printer settings were adjusted for the best print quality, which ejected the largest volume of ink onto the substrate. Patterns for inkjet printing were quickly and easily designed using Auto CAD. Printing of the Ag–MWCNT ink was performed on paper. The Ag–MWCNT ink was printed different times to observe the relationship between the sheet resistance and the number of prints. MnO_2 nanoparticles were added into the Ag–MWCNT ink and the anode was printed by the same method as that used for the above conductive patterns. The vacuum filtration method was used to fabricate the MWCNT film cathode. MWCNTs were added into 40 ml distilled water with different masses (18 mg, 20 mg, and 25 mg). Then 20 mg SDBS, used as a surfactant, was dissolved in the above solution and then stirred for 30 min, at last 30 min probe ultrasonication was adopted to further form a uniform solution. The as-obtained solution was filtered through a membrane (450 nm pore size). The obtained filter cake was dried at room temperature for 24 h.

Assembly of MnO_2–Ag–MWCNT/MWCNT ASCs

An ASC with aqueous electrolyte was assembled using a piece of MnO_2–Ag–MWCNT (1×1 cm^2) and a piece of MWCNT film (1×1 cm^2), with an electrolyte-soaked (4 M LiCl) separator in between. Adhesive tape was used to seal the ASCs.

Characterization

The morphologies and elements of printed conductive patterns were observed and analyzed with a scanning electron microscope (SEM, FEI Nova Nano-SEM 450) The XRD patterns of the samples were recorded by X-ray diffraction (XRD, PANalytical B.V. X'Pert PRO). To investigate the flexibility of the electrodes, a three-dimensional (3D) mechanical stage was used to apply a strain on the free end of the sample, with the other end fixed tightly on a manipulation holder. The compressing process is illustrated in ESI Fig. S1.† The different slope of the I–V curves which means the resistance of conductive films corresponds to different external compressive strains. Electrochemical measurements including galvanostatic charge–discharge (GCD), cyclic voltammetry (CV), electrochemical impedance spectroscopy (EIS, 100 kHz to 0.01 Hz) were conducted on an electrochemical workstation (CHI 660E). The electrochemical performance of individual electrodes was tested using a three-electrode system with a 4 M LiCl solution serving as an electrolyte, a platinum electrode and Ag/AgCl were used as a counter electrode and reference electrode prior to the fabrication of ASCs, respectively. The performance of ASCs was measured using a two-electrode configuration.

Results and discussion

The fabrication of conductive patterns and patterned anodes is illustrated in Fig. 1a. A personal computer was used to design conductive patterns which were then inkjet-printed using a home printer. The concentration of the ink is important for inkjet printing, because too high concentration will clog the nozzle, and too low concentration will increase the printing times to acquire the appropriate electrodes. For this reason, 5 mg ml^{-1} MWCNTs and 4 mg ml^{-1} Ag were chosen for the printed ink. The photos of the ink are shown in Fig. 1b. The mixtures of the ink dispersed well, and there was no obvious

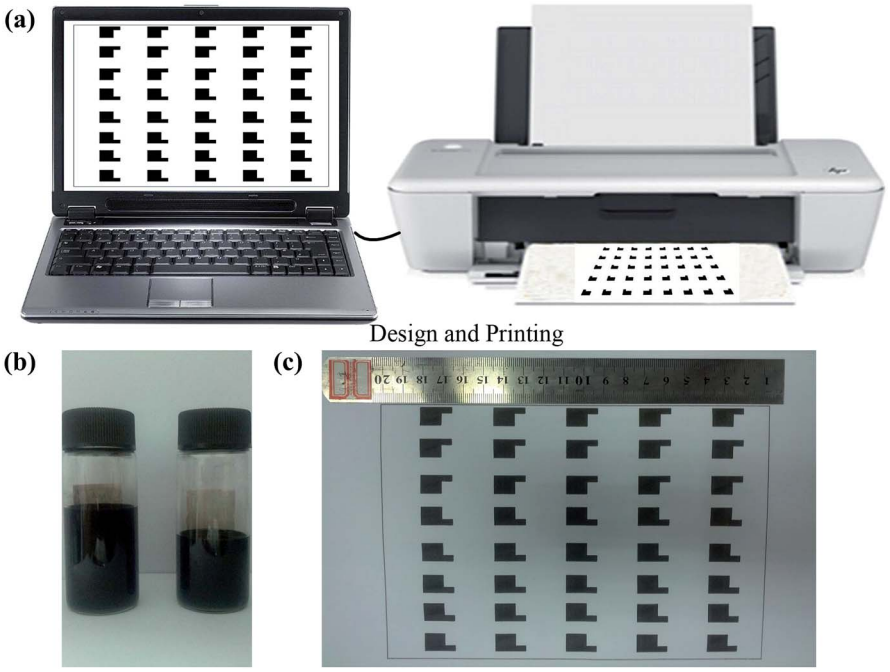

Fig. 1 Overview of the fabrication process for inkjet-printing: (a) design using a personal computer and inkjet-printing using a home printer. (b) The well-dispersed ink for inkjet-printing. (c) A photo of patterned electrodes.

precipitation even after a long time. Fig. 1c shows the photograph of inkjet-printed conductive patterns.

The XRD patterns of the as-prepared samples are presented in ESI Fig. S2a.† The samples were poorly crystallized and a broad peak at 37.5° can be clearly observed. This can be ascribed to the (211) diffraction peak of α-MnO_2 (ICDD-JCPDS Card no. 44-0141). The diameter of MnO_2 nanoparticles was 60–90 nm (ESI Fig. S2b†). The morphologies of patterned electrodes are shown in Fig. 2a and b. Ag and MnO_2 nanoparticles are distributed around the MWCNTs and have a tight connection with MWCNTs. The ejected MWCNTs formed tangled, dense, and homogeneous networks and tightly located on the paper fiber (ESI Fig. S2c and d†). The thickness of the printed Ag–MWCNT conductive pattern and the MnO_2–Ag–MWCNT

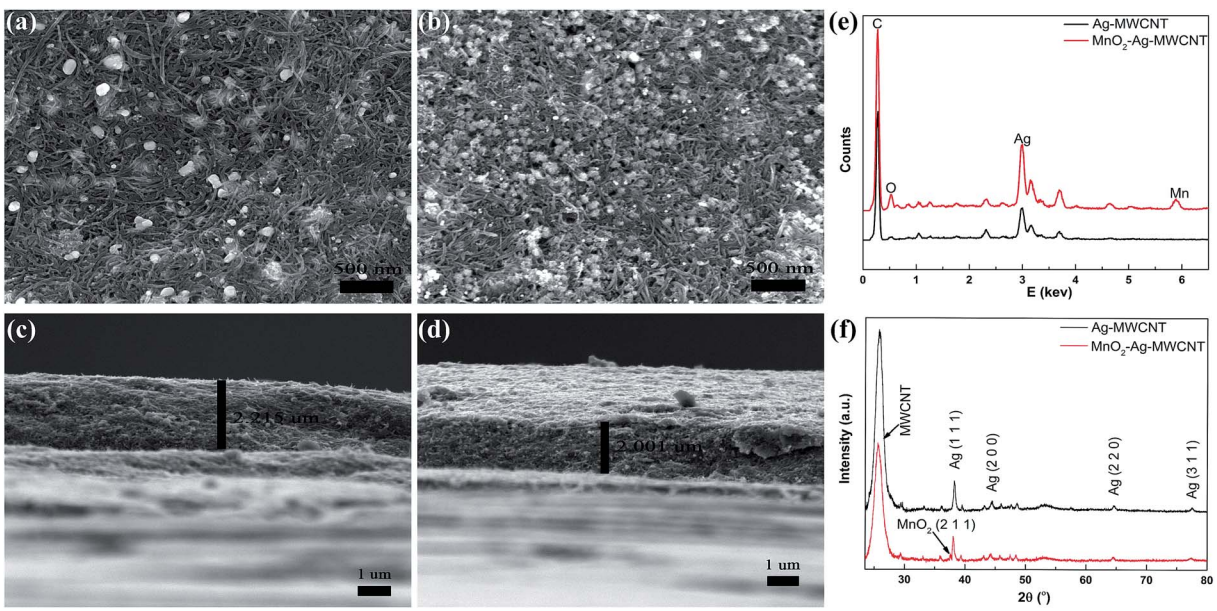

Fig. 2 SEM images of (a) printed Ag–MWCNT conductive pattern and (b) printed MnO_2–Ag–MWCNT patterned positive electrode. The side view of (c) Ag–MWCNT and (d) MnO_2–Ag–MWCNT on paper substrates. (e) EDS of printed Ag–MWCNT and MnO_2–Ag–MWCNT. (f) XRD patterns of Ag–MWCNT and MnO_2–Ag–MWCNT.

patterned anode is 2.215 μm and 2.001 μm and is indicated in Fig. 2c and d, respectively. The filtrated MWCNTs for the cathode were also tightly tangled, and the thickness was 12.05 μm (see ESI Fig. S2e and f†). In order to confirm the ingredients of the Ag–MWCNT conductive patterns and MnO_2–Ag–MWCNT patterned anodes, EDX and XRD analyses were used, as shown in Fig. 2e and f. The EDS spectrum confirmed that the C and Ag signals were from the Ag–MWCNT conductive patterns (black line) and Mn, an increased peak of O came from the patterned anodes (red line). The other peak came from paper substrates (ESI Fig. S3a†). XRD patterns showed that the peaks of MWCNTs at 26°, 38.1°, 44.3°, 64.5°, and 77.4° were attributed to the diffraction of (111), (200), (220), (311) crystalline planes of the face-centered structure of Ag (black line). The peak at 37.5° came from (211) of MnO_2 (red line), as shown clearly in ESI Fig. S3b.† Other peaks came from paper substrates (ESI Fig. S3c†).

Both Ag–MWCNT ink and MWCNT ink were used to inkjet conductive patterns. The electrical resistance was rapidly reduced with the increasing number of overprinting. It was also observed that adding Ag nanoparticles will significantly improve the conductivity (Fig. 3a), which is mainly due to the good conductivity of Ag nanoparticles and good connection between Ag and MWCNTs. After being printed 50 times, the conductive pattern fabricated by Ag–MWCNT ink reaches a sheet resistance as low as 300 Ω sq^{-1}, which is much lower than those reported in the literature.[43,44] For further characterizing the stability, we defined curvature as the bended chord height of total length divided by the total length ($C = H/L$, see Fig. 3b inset). Fig. 3b shows the changes in sheet resistance expressed as $(R - R_0)/R_0$, where R_0 is the initial sheet resistance and R is the sheet resistance after bending as a function of curvature. During bending, the changes of sheet resistance were random mainly due to the random connection between Ag and MWCNTs. However, the changes did not exceed 25% all the time. After we bend the electrode with a 20% curvature 2000 times, the changes of sheet resistance were no more than 10% (Fig. 3c). The inset demonstrates a foldable electric circuit by operating a LED on paper with the Ag–MWCNT electrode. The conductive patterns may have potential applications in flexible/foldable optoelectronic devices.

To explore the potential applications in energy storage, the as-printed Ag–MWCNT electrode (mass density of 0.738 mg cm^{-2}) and MnO_2–Ag–MWCNT electrode (mass density of 1.218 mg cm^{-2}) were characterized by CV, GCD and EIS measurements. Fig. 4a and b present CV curves of the anodes with scanning rates from 2 mV s^{-1} to 1 V s^{-1}. As expected, the electrode showed ideal capacitive behavior with rectangular CV curves (Fig. 4a). The electrodes containing MnO_2 exhibited substantially larger current density than Ag–MWCNT electrodes (Fig. 4c) because MnO_2 is more electrochemically active than MWCNTs. As shown in Fig. 4d, the GCD performance was further tested. The charge–discharge time of the MnO_2–Ag–MWCNT system was actually prolonged, by 328% compared to the Ag–MWCNT system at the same current of 0.1 mA, indicating a great enhancement in supercapacitance. The volumetric capacitance (see Fig. 4e) was evaluated by the above CV results, which decreased with the scanning rate. At a scan rate of 10 mV s^{-1}, the volumetric capacitance of the MnO_2–Ag–MWCNT electrode was 30.5 F cm^{-3}, about 5 times larger than that of the Ag–MWCNT electrode. Even at a scan rate of 1 V s^{-1}, the volumetric capacitance of the MnO_2–Ag–MWCNT electrode was 4.1 F cm^{-3}. The EIS data were analyzed using the Nyquist plot. The intercept of the plot at the *X*-axis represents the equivalent series resistance (ESR) of the electrode which determines the charge–discharge rate of the electrode.[45] Fig. 4f shows the Nyquist plot of the electrodes, the ESR values of the Ag–MWCNT electrode (27.3 Ω) and the MnO_2–Ag–MWCNT electrode (8.1 Ω). The charge transfer resistances of the Ag–MWCNT electrode and MnO_2–Ag–MWCNT electrode were 188.5 and 85.6 Ω, respectively (ESI Fig. S4†), which implied that adding MnO_2 nanoparticles would not increase the resistance of the electrodes. The densities of the Ag–MWCNT electrode and MnO_2–Ag–MWCNT electrode were 0.333 and 0.609 g cm^{-3}, respectively. Higher density means tighter connections between different MWCNTs and MWCNT/Ag, and more beneficial for the electron transfer. It is well known that charge balance between positive and negative electrodes is crucial to maximize the

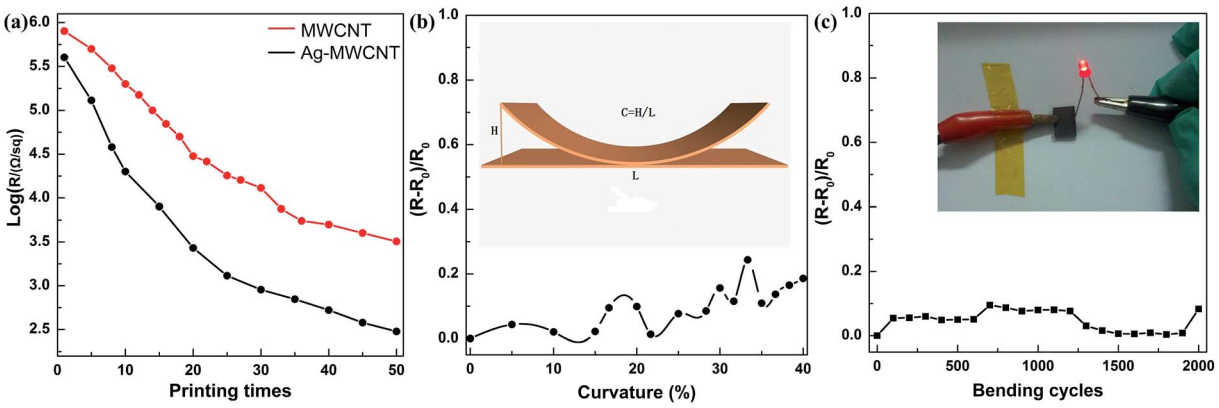

Fig. 3 (a) Logarithm of sheet resistance *versus* the number of prints. (b) Changes in the electrical resistance of conductive patterns *vs.* curvature. (c) Changes in the electrical resistance of conductive patterns *vs.* bending cycles, the inset shows a foldable circuit by operating a LED on paper with the Ag–MWCNT electrode.

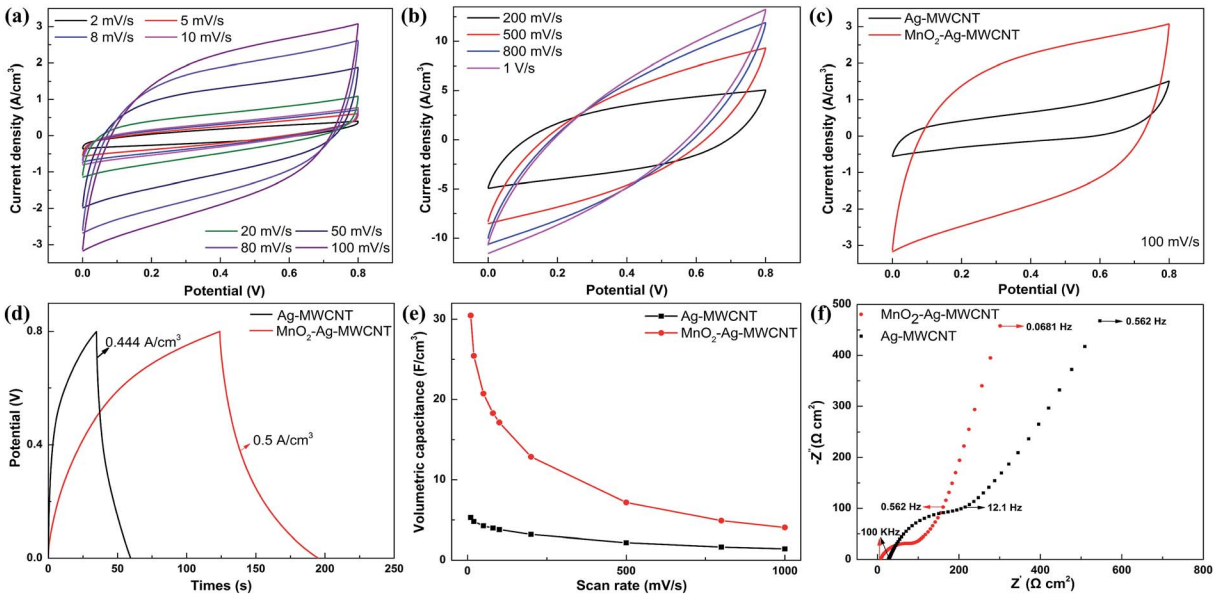

Fig. 4 Electrochemical performance of the Ag–MWCNT and MnO_2–Ag–MWCNT electrodes. Cyclic voltammograms of the MnO_2–Ag–MWCNT electrodes with scan rate (a) from 0.001 V s^{-1} to 0.1 V s^{-1} and (b) from 0.2 V s^{-1} to 1 V s^{-1}. (c) Cyclic voltammograms of the Ag–MWCNT and MnO_2–Ag–MWCNT electrodes at a scan rate of 0.1 V s^{-1}. (d) Galvanostatic charge–discharge behavior of the electrodes with 0.444 A cm^{-3} and 0.5 A cm^{-3}, respectively. (e) Volumetric capacitance *vs.* scan rate for the electrodes. (f) Nyquist plot of the electrodes.

energy density of ASCs.[46] So MWCNTs with different masses were filtrated. The capacitance of the MWCNT film with a mass density of 1.315 mg cm^{-2} was the most close to positive electrodes at a scanning rate of 100 mV s^{-1} (ESI Fig. S5a†). We chose the filtrated MWCNT membranes (1.315 mg cm^{-2}) to fabricate our cathodes. The cathodes showed ideal capacitive behaviour with rectangular and symmetry CV curves (ESI Fig. S5b†). The volumetric capacitance reached 5.3 F cm^{-3} at a scanning rate of 10 mV s^{-1} and the ESR was 16.5 Ω (ESI Fig. S5c and d†).

To further investigate the performances of the asymmetric supercapacitor fabricated with the inkjet-printed anode and well-matched cathode, a variety of electrochemical measurements have been performed using two electrode configurations. The CV measurements indicated that the device exhibited a stable potential window up to 1.8 V (Fig. 5a). The large potential

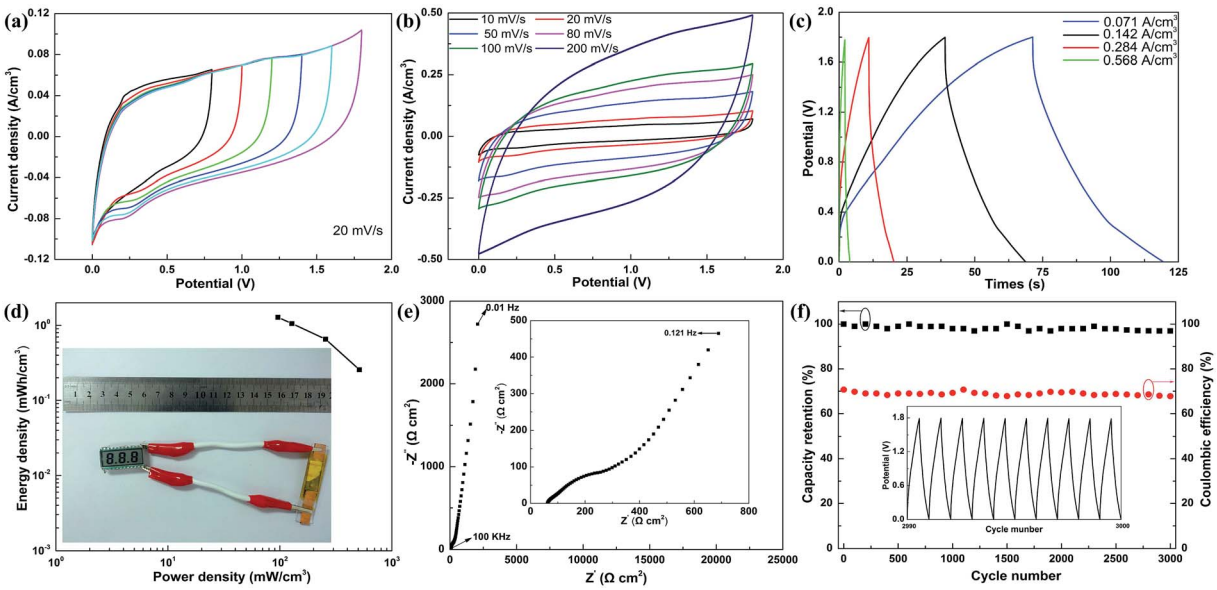

Fig. 5 Electrochemical performances of the ASC. (a) CV curves of the device in different potential windows, the scan rate is 20 mV s^{-1}. (b) CV curves of the device at different scan rates. (c) Galvanostatic discharge curves of the device at different current densities. (d) Energy and power density plot. (e) Nyquist plot. (f) Cycle life and coulombic efficiency, inset shows the GCD curve from 2990th to 3000th cycles.

window means a high energy density, which is a major advantage compared to common symmetric supercapacitors and a very important factor to meet the demand of application. As shown in Fig. 5b, the asymmetric supercapacitor had well symmetrical and near rectangular CV curves in a potential window of 0–1.8 V, indicating that the device also had good capacitance performance. Good linear profiles of GCD curves with different current densities (Fig. 5c) further confirm the perfect electrochemical behaviour of the device. The asymmetric supercapacitor showed a high energy density of 1.28 mW h cm^{-3} at a power density of 96 mW cm^{-3}. Moreover, a high power density of 512.1 mW cm^{-3} was obtained, and the energy density was still as high as 0.256 mW h cm^{-3} at a discharge current density of 0.568 A cm^{-3}. A commercial liquid crystal display was successfully driven by the ASC after being fully charged (Fig. 5d). Fig. 5e presents the impedance spectrum of the as-fabricated device which exhibits a negligible 45° Warburg region and the ESR value (61.8 Ω) of the device, indicating the fast ion transport at the active material–electrolyte interface. The impedance spectrum becomes almost a vertical line where the imaginary part of impedance increases dramatically in the low frequency range, showing the perfect capacitive behaviour of ion diffusion in the electrode materials. GCD at a current density of 0.142 A cm^{-3} for 3000 cycles was carried out to evaluate the long-term cycle stability (as shown in Fig. 5f). The capacitance only had a slight fluctuation in the whole process. The capacity retention is 96.9% after 3000 cycles and the coulombic efficiency was kept almost the same. This implied the good charge–discharge reversibility of the device.

Conclusions

Highly conductive patterns by inkjet-printing have been successfully prepared. By adding Ag nanoparticles to MWCNT ink, the sheet resistance of the patterns decreased to 300 Ω sq^{-1} after being printed 50 times. The conductive patterns could act as a foldable electric circuit. MnO_2–Ag–MWCNT anodes were also fabricated by inkjet printing. An asymmetric supercapacitor was fabricated by assembling an inkjet-printed MnO_2–Ag–MWCNT anode with a filtrated MWCNT cathode. The supercapacitor has a wide operating potential window of 1.8 V and exhibits excellent electrochemical performance, *e.g.*, a high density of 1.28 mW h cm^{-3} at a power density of 96 mW cm^{-3} and a high retention ratio of ~96.9% of its initial capacitance after 3000 cycles. The inkjet-printing acting as a simple, low-cost, non-contact deposition method can be fully integrated with the fabrication process in current printed electronic devices and has potential applications in energy storage.

Acknowledgements

This work was supported by the National Basic Research program (2011CB933300) of China, the National Natural Science Foundation of China (11204093, 11374110), the Overseas Master Program (MS2011HZKJ043), and the Fundamental Research Funds for the Central Universities (HUST: 2014TS124 and 2013TS033). Y. H. G. would like to thank Prof. Zhong-Lin Wang for the support of experimental facilities in WNLO of HUST.

Notes and references

1 Y. Chen, J. Au, P. Kazlas, A. Ritenour, H. Gates and M. McCreary, *Nature*, 2003, **423**, 136.
2 A. Rida, L. Yang, R. Vyas and M. M. Tentzeris, *IEEE Antenn. Propag. Mag.*, 2009, **51**, 13–23.
3 L. Huang, Y. Huang, J. J. Liang, X. J. Wan and Y. S. Chen, *Nano Res.*, 2011, **4**, 675–684.
4 V. Marin, E. Holder, M. M. Wienk, E. Tekin, D. Kozodaev and U. S. Schubert, *Macromol. Rapid Commun.*, 2005, **26**, 319–324.
5 G. Orecchini, F. Alimenti, V. Palazzari, A. Rida, M. M. Tentzeris and L. Roselli, *IET Microwaves, Antennas & Propagation*, 2011, **5**, 993–1001.
6 D. Pech, M. Brunet, P. L. Taberna, P. Simon, N. Fabre, F. Mesnilgrente, V. Conedera and H. Durou, *J. Power Sources*, 2010, **195**, 1266–1269.
7 J. G. Ok, M. K. Kwak, C. M. Huard, H. S. Youn and L. J. Guo, *Adv. Mater.*, 2013, **25**, 6554–6561.
8 B. Schumm, F. M. Wisser, G. Mondin, F. Hippauf, J. Fritsch, J. Grothe and S. Kaskel, *J. Mater. Chem. C*, 2013, **1**, 638–645.
9 J. Jang, Y. Song, H. Oh, D. Yoo, D. Kim, H. Lee, S. Hong, J. K. Lee and T. Lee, *Appl. Phys. Lett.*, 2014, **104**, 053301.
10 A. Chiolerio, M. Cotto, P. Pandolfi, P. Martino, V. Camarchia, M. Pirola and G. Ghione, *Microelectron. Eng.*, 2012, **97**, 8–15.
11 T. Shimoda, Y. Matsuki, M. Furusawa, T. Aoki, I. Yudasaka, H. Tanaka, H. Iwasawa, D. H. Wang, M. Miyasaka and Y. Takeuchi, *Nature*, 2006, **440**, 783–786.
12 Y. Y. Noh, X. Y. Cheng, H. Sirringhaus, J. I. Sohn, M. E. Welland and D. J. Kang, *Appl. Phys. Lett.*, 2007, **91**, 043109.
13 M. B. Madec, P. J. Smith, A. Malandraki, N. Wang, J. G. Korvink and S. G. Yeates, *J. Mater. Chem.*, 2010, **20**, 9155–9160.
14 D. H. Lee, S. Y. Han, G. S. Herman and C. H. Chang, *J. Mater. Chem.*, 2009, **19**, 3135–3137.
15 G. Mauthner, K. Landfester, A. Kock, H. Bruckl, M. Kast, C. Stepper and E. J. W. List, *Org. Electron.*, 2008, **9**, 164–170.
16 D. Angmo, J. Sweelssen, R. Andriessen, Y. Galagan and F. C. Krebs, *Adv. Energy Mater.*, 2013, **3**, 1230–1237.
17 Y. Y. Sun, Y. J. Zhang, Q. Liang, Y. Zhang, H. J. Chi, Y. Shi and D. N. Fang, *RSC Adv.*, 2013, **3**, 11925–11934.
18 W. Voit, W. Zapka, L. Belova and K. V. Rao, *IEE Proc.-A:Sci., Meas. Technol.*, 2003, **150**, 252–256.
19 P. Tiberto, G. Barrera, F. Celegato, M. Coisson, A. Chiolerio, P. Martino, P. Pandolfi and P. Allia, *Eur. Phys. J. B*, 2013, **86**, 173.
20 E. Katzir, S. Yochelis, Y. Paltiel, S. Azoubel, A. Shimoni and S. Magdassi, *Sens. Actuators, B*, 2014, **196**, 112–116.
21 X. Liu, L. L. Gu, Q. P. Zhang, J. Y. Wu, Y. Z. Long and Z. Y. Fan, *Nat. Commun.*, 2014, **5**, 4007.
22 A. Chiolerio, S. Bocchini and S. Porro, *Adv. Funct. Mater.*, 2014, **24**, 3375–3383.
23 L. S. Fan, N. Q. Zhang and K. N. Sun, *Chem. Commun.*, 2014, **50**, 6789–6792.

24 H. Pan, J. Y. Li and Y. P. Feng, *Nanoscale Res. Lett.*, 2010, **5**, 654–668.
25 J. W. Song, J. Kim, Y. H. Yoon, B. S. Choi, J. H. Kim and C. S. Han, *Nanotechnology*, 2008, **19**, 095702.
26 T. Kim, H. Song, J. Ha, S. Kim, D. Kim, S. Chung, J. Lee and Y. Hong, *Appl. Phys. Lett.*, 2014, **104**, 113103.
27 R. P. Tortorich, E. Song and J. W. Choi, *J. Electrochem. Soc.*, 2014, **161**, B3044–B3048.
28 A. Shimoni, S. Azoubel and S. Magdassi, *Nanoscale*, 2014, **6**, 11084–11089.
29 L. B. Hu, H. S. Kim, J. Y. Lee, P. Peumans and Y. Cui, *ACS Nano*, 2010, **4**, 2955–2963.
30 A. Chiolerio, G. Maccioni, P. Martino, M. Cotto, P. Pandolfi, P. Rivolo, S. Ferrero and L. Scaltrito, *Microelectron. Eng.*, 2011, **88**, 2481–2483.
31 L. Li, Y. Guo, X. Zhang and Y. Song, *J. Mater. Chem. A*, 2014, **2**, 19095–19101.
32 Q. Li, Z. L. Wang, G. R. Li, R. Guo, L. X. Ding and Y. X. Tong, *Nano Lett.*, 2012, **12**, 3803–3807.
33 L. Y. Yuan, X. H. Lu, X. Xiao, T. Zhai, J. J. Dai, F. C. Zhang, B. Hu, X. Wang, L. Gong, J. Chen, C. G. Hu, Y. X. Tong, J. Zhou and Z. L. Wang, *ACS Nano*, 2012, **6**, 656–661.
34 X. Xiao, T. P. Ding, L. Y. Yuan, Y. Q. Shen, Q. Zhong, X. H. Zhang, Y. Z. Cao, B. Hu, T. Zhai, L. Gong, J. Chen, Y. X. Tong, J. Zhou and Z. L. Wang, *Adv. Energy Mater.*, 2012, **2**, 1328–1332.
35 C. Guan, J. P. Liu, C. W. Cheng, H. X. Li, X. L. Li, W. W. Zhou, H. Zhang and H. J. Fan, *Energy Environ. Sci.*, 2011, **4**, 4496–4499.
36 J. Y. Tao, N. S. Liu, W. Z. Ma, L. W. Ding, L. Y. Li, J. Su and Y. H. Gao, *Sci. Rep.*, 2013, **3**, 2286.
37 J. Liu, L. Zhang, H. B. Wu, J. Lin, Z. Shen and X. W. Lou, *Energy Environ. Sci.*, 2014, 3709–3719.
38 N. S. Liu, W. Z. Ma, J. Y. Tao, X. H. Zhang, J. Su, L. Y. Li, C. X. Yang, Y. H. Gao, D. Golberg and Y. Bando, *Adv. Mater.*, 2013, **25**, 4925–4931.
39 M. Toupin, T. Brousse and D. Belanger, *Chem. Mater.*, 2004, **16**, 3184–3190.
40 J. Yan, Z. J. Fan, W. Sun, G. Q. Ning, T. Wei, Q. Zhang, R. F. Zhang, L. J. Zhi and F. Wei, *Adv. Funct. Mater.*, 2012, **22**, 2632–2641.
41 X. Xiao, T. Li, Z. Peng, H. Jin, Q. Zhong, Q. Hu, B. Yao, Q. Luo, C. Zhang, L. Gong, J. Chen, Y. Gogotsi and J. Zhou, *Nano Energy*, 2014, **6**, 1–9.
42 R. Jiang, T. Huang, Y. Tang, J. Liu, L. Xue, J. Zhuang and A. Yu, *Electrochim. Acta*, 2009, **54**, 7173–7179.
43 K. Kordas, T. Mustonen, G. Toth, H. Jantunen, M. Lajunen, C. Soldano, S. Talapatra, S. Kar, R. Vajtai and P. M. Ajayan, *Small*, 2006, **2**, 1021–1025.
44 O.-S. Kwon, H. Kim, H. Ko, J. Lee, B. Lee, C.-H. Jung, J.-H. Choi and K. Shin, *Carbon*, 2013, **58**, 116–127.
45 M. D. Stoller, S. J. Park, Y. W. Zhu, J. H. An and R. S. Ruoff, *Nano Lett.*, 2008, **8**, 3498–3502.
46 J. P. Zheng, *J. Electrochem. Soc.*, 2003, **150**, A484–A492.